DOI: 10.1002/cphc.200900298

Influence of Intermolecular Vibrations on the Electronic Coupling in Organic Semiconductors: The Case of Anthracene and Perfluoropentacene

Nicolas G. Martinelli,[a, b] Yoann Olivier,[a] Stavros Athanasopoulos,[a] Mari-Carmen Ruiz Delgado,[b] Kathryn R. Pigg,[b] Demétrio A. da Silva Filho,[b] Roel S. Sánchez-Carrera,[b] Elisabetta Venuti,[c] Raffaele G. Della Valle,[c] Jean-Luc Brédas,[a, b] David Beljonne,[a, b] and Jérôme Cornil*[a, b]

We have performed classical molecular dynamics simulations and quantum-chemical calculations on molecular crystals of anthracene and perfluoropentacene. Our goal is to characterize the amplitudes of the room-temperature molecular displacements and the corresponding thermal fluctuations in electronic transfer integrals, which constitute a key parameter for charge transport in organic semiconductors. Our calculations show that the thermal fluctuations lead to Gaussian-like distributions of the transfer integrals centered around the values obtained for the equilibrium crystal geometry. The calculated distributions have been plugged into Monte-Carlo simulations of hopping transport, which show that lattice vibrations impact charge transport properties to various degrees depending on the actual crystal structure.

1. Introduction

The charge-transport mechanisms in organic semiconductors are not fully understood yet, although charge-carrier mobilities play a critical role in determining the performance of organic electronic devices. In the case of highly ordered systems (i.e. molecular crystals of high purity at very low temperature) with strong electronic coupling, charge transport operates in the band regime.[1] In this instance, the charge-carrier wavefunctions are delocalized and the carrier mobility decreases with temperature as a result of scattering induced by phonons, as observed in crystalline inorganic semiconductors (scattering gradually leads to carrier localization). In disordered materials, charge transport takes place in the (incoherent) hopping regime;[2] the charge-carrier wavefunctions are then localized on a single (or a few) molecules as a result of energetic and/or spatial disorder. It is much less straightforward to assess the actual charge transport mechanism in a molecular crystal at room temperature as it often lies in the cross-over region between the band and hopping regimes, which turns out to be difficult to model.[3]

In this context, recent theoretical work by Troisi and coworkers based on phenomenological models involving realistic parameters for crystalline organic semiconductors confirms that in general the coherence of electronic bands is lost at room temperature due to thermal activation of lattice phonons, that is through, intermolecular vibrational modes.[4–6] As intra-molecular and inter-molecular vibrations break the symmetry of the equilibrium crystal structure, they lead to carrier localization as a result of thermal fluctuations in:

1) transfer integrals, which describe the strength of the electronic couplings between adjacent molecules.[7] The modulation of the transfer integrals by vibrations is referred to as nonlocal electron-phonon coupling; and

2) site energies (i.e. roughly speaking, the energies of the HOMO or LUMO levels in the case of hole transport or electronic transport, respectively). This is referred to as local electron-phonon coupling.

It is useful to point out that phenomenological models can hardly grasp the intricacies of such processes.

In recent years, much work has been devoted to the understanding of the impact of chemical structure and molecular packing on the electronic coupling between adjacent molecules.[8] Model calculations have highlighted the extreme sensitivity of the transfer integrals on longitudinal and lateral displacements of adjacent molecules and their rotations. Thus, gaining a deeper understanding of charge transport requires

[a] N. G. Martinelli, Dr. Y. Olivier, Dr. S. Athanasopoulos, Prof. J.-L. Brédas, Dr. D. Beljonne, Dr. J. Cornil
Chemistry of Novel Materials
University of Mons, Place du Parc 20, 7000 Mons (Belgium)
Fax: (+32) 65373861
E-mail: Jerome@averell.umh.ac.be

[b] N. G. Martinelli, Dr. M.-C. Ruiz Delgado, K. R. Pigg, Dr. D. A. da Silva Filho, Dr. R. S. Sánchez-Carrera,[#] Prof. J.-L. Brédas, Dr. D. Beljonne, Dr. J. Cornil
School of Chemistry and Biochemistry
Georgia Institute of Technology
901 Atlantic Drive NW, Atlanta, GA 30332-0400 (USA)

[c] E. Venuti, Prof. R. G. Della Valle
Dipartimento di Chimica Fisica e Inorganica
Università di Bologna, Viale Risorgimento 4, 40136 Bologna (Italy)

[#] Current address:
Harvard University, Department of Chemistry and Chemical Biology
12 Oxford Street, Cambridge, Massachusetts 02138 (USA)

that the modulation of the transfer integrals by the lattice dynamics be suitably taken into account.[9] The key role played by intermolecular vibrations in defining the charge transport properties has also been evidenced in previous theoretical studies addressing the temperature dependence of charge mobilities in molecular crystals.[10,11] In these investigations, the impact of a given intermolecular mode has been introduced via a non-local electron-phonon coupling (related to the derivatives at various orders of the transfer integral along this mode).

Since hopping of a charge between adjacent molecules can be viewed as an electron-transfer reaction, quantum-chemical approaches have been recently developed in the framework of Marcus theory[12] to estimate the molecular parameters governing the charge hopping rate between two adjacent molecules. The perturbative Marcus expressions provide a square dependence of the electron-transfer rates on the transfer integrals and can be extended to incorporate polaronic, polarization, and electric-field effects.[13] A simple way to estimate charge mobilities is then to inject the Marcus rates into Monte Carlo simulations (thus assuming that a weak coupling regime is valid) and to propagate the charge carriers in supramolecular assemblies.[14,15] This particular approach has been applied most often to static lattices or to an ensemble of snapshots extracted from MD simulations (see ref. [16] and references therein).

Previous theoretical studies on donor-bridge-acceptor molecules have also shown that dynamic fluctuations can significantly modulate the amplitude of electronic couplings for intramolecular electron transfer.[17] This has been further illustrated by Troisi and co-workers in the case of molecular crystals by combining molecular dynamics (MD) calculations, which depict the intermolecular vibrational modes, with quantum-chemical calculations performed on a large number of MD snapshots, which allow access to the electronic properties. Note that the main advantage of MD simulations is to encompass all vibrational modes of the system instead of the few *effective* modes usually considered in phenomenological models. When applied to rubrene and pentacene,[4–6] this approach yields a quasi-Gaussian distribution of the transfer integrals. Importantly, in a number of instances, the standard deviation is found to be as large as the value of the transfer integral obtained for the equilibrium crystal geometry.[18] Thus, a key step for improving the description of charge transport in molecular crystals is to determine the distribution of transfer integrals induced by lattice vibrations for given pairs of molecules.

The goal of the present work is to apply a procedure similar to that developed by Troisi and co-workers: i) to determine for various structures the actual molecular displacements at room temperature and the resulting thermal fluctuations in the amplitude of the transfer integrals; and ii) to assess the influence of lattice dynamics on charge carrier mobilities calculated in a hopping regime using kinetic Monte Carlo simulations. By considering selected examples, we find that lattice vibrations generally induce the expected Gaussian broadening of the transfer integrals and a modulation of the charge transport properties (compared to the values computed for the equilibrium crystal geometry) whose extent depends on the width and location of the centre of the Gaussian distribution as well as on the relative timescales of the lattice vibration and charge transfer processes.

2. Theoretical Methodology

For the sake of illustration, we have considered here the crystals of anthracene and perfluoropentacene, see Figure 1. The main reason behind this choice is that these crystals provide

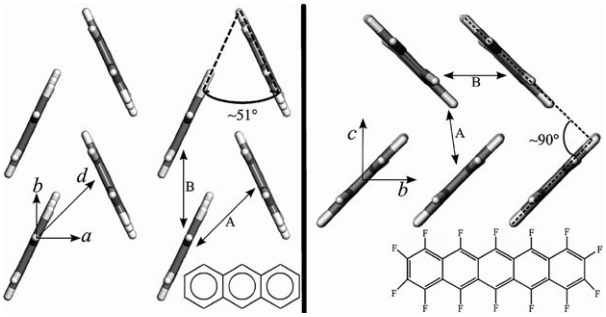

Figure 1. Representation of the crystal unit cell of anthracene (left) and fluorinated pentacene (right); the chemical structure of the two molecules and the labeling of the different dimers are also displayed.

for a variety of transfer integral distributions at room temperature. Anthracene crystallizes in the monoclinic space group C_2h_5 ($P2_1/a$),[19] with molecules packing into a herringbone structure (the herringbone angle is 51° in the experimental X-ray structure and 47° at the molecular mechanics (MM) level with the COMPASS force field, see Figure 1); the centrosymmetric unit cell contains two inequivalent molecules. The factor group analysis of the $k=0$ lattice modes yields six Raman active librational modes (of symmetry $3A_g + 3B_g$), three infrared-active translational modes ($2A_u + B_u$), and three inactive acoustic modes ($A_u + 2B_u$).[20]

In the equilibrium crystal geometry optimized with the COMPASS force field (vide infra), significant transfer integrals are calculated at the semi-empirical Hartree–Fock INDO (intermediate neglect of differential overlap) level only along the *b* axis ($t_{hole}=44$ meV; $t_{electron}=26$ meV) and along the diagonal *d* axis ($t_{hole}=34$ meV; $t_{electron}=45$ meV). The transfer integrals are vanishingly small between molecules located in adjacent layers, which suggests that transport in this material is anisotropic. Note that the INDO method has been chosen for the evaluation of the transfer integrals in this study since: i) it generally yields very good quantitative agreement when compared to results obtained with first-principles Hartree–Fock or DFT (density functional theory) calculations;[13] ii) it would be prohibitive to compute at the ab initio level the transfer integrals for thousands of snapshots extracted from MD runs with the goal of extending this approach to more amorphous materials; and iii) the transfer integrals can be directly estimated from the electronic matrix elements between two molecules (and, thus, are not calculated on the basis of an energy-splitting-in-dimer approach that can be biased by spurious polari-

zation effects).[21,22] This is done by expanding the molecular orbitals ϕ_1 and ϕ_2 of the individual molecules into atomic contributions as shown in Equation (1):

$$V_{if} = \langle \phi_1 | h | \phi_2 \rangle = \sum_{\mu} \sum_{\nu} C_{1\mu} C_{2\nu} \langle \chi_\mu | h | \chi_\nu \rangle \quad (1)$$

where $C_{1\mu}$ ($C_{2\nu}$) corresponds to the LCAO (linear combination of atomic orbitals) coefficient of atomic orbital χ_μ (χ_ν) in molecular orbital ϕ_1 (ϕ_2). The matrix element $<\chi_\mu | h | \chi_\nu>$ is implemented in the INDO method as Equation (2):

$$\langle \chi_\mu | h | \chi_\nu \rangle = \frac{1}{2}(\beta_A + \beta_B) S_{\mu\nu} \quad (2)$$

where β_A and β_A are two parameters depending on the nature of atoms *A* and *B*, $S_{\mu\nu}$ is the overlap factor between the atomic orbitals χ_μ and χ_ν corrected by empirical factors.[23]

The perfluoropentacene crystal belongs to the monoclinic C_2h_5 ($P2_1/c$) space group, and its primitive unit cell is defined by two inequivalent molecules.[24] As for anthracene and many other oligoacene-based molecular crystals, the crystal features a herringbone packing (with a herringbone angle of 91° in the experimental X-ray structure and 79° at the MM level with the COMPASS force field, see Figure 1). According to crystal symmetry, the same lattice vibrations as in anthracene are present at $k=0$.[25] In the equilibrium perfluoropentacene crystal geometry provided by COMPASS, substantial transfer integrals are calculated at the INDO level along the *b* axis ($t_{hole}=156$ meV; $t_{electron}=127$ meV) while very small values are obtained along the *c* axis ($t_{hole}=4$ meV; $t_{electron}=1$ meV). This would imply quasi-one-dimensional transport when neglecting the impact of lattice dynamics.

The use of a classical approach to describe the nonlocal electron-phonon coupling in molecular crystals at room temperature has been recently validated in the case of naphthalene through a direct comparison with results obtained by treating the intermolecular modes quantum-mechanically.[18] In order to describe the lattice dynamics at the MD level, the first step is to carefully select a force field that yields lattice parameters for the unit cell comparable to available experimental X-ray data. Our procedure is to run a MD calculation (in the NVT ensemble at 300 K with a timestep of 1 fs) starting from the experimental crystal structure and to minimize several geometries along the trajectory to make sure that a unit cell similar to the experimental one is constantly recovered. This selection procedure has been verified successfully when using COMPASS[26] for both anthracene and perfluoropentacene. This procedure ensures that the crystal vibrates around the experimental crystal structure in the course of the simulations. Note that, in contrast, the widely used UFF (universal force field)[27] fails to reproduce the global minimum of anthracene. Table 1 collects the lattice parameters of the unit cell for the two molecular crystals, as provided by the COMPASS force field and experimental X-ray diffraction spectra. There is very good quantitative agreement between the two sets of data in the case of anthracene while larger deviations are obtained for perfluoropentacene. However, for the latter, the key point that we will address in the following is the very small transfer integral obtained for electrons along the *c* axis, a feature which is reproduced when starting from both the X-ray structure or the COMPASS geometry. Another check for the consistency of the COMPASS force field for anthracene was achieved by comparing the frequencies of the nine intermolecular optical modes of the anthracene unit cell with corresponding quantum-chemical calculations performed at the DFT level with the B3LYP functional. Table 2 collects the results and points to a very good quantitative agreement between the two sets of data; this further validates the use of the COMPASS force field. The DFT-calculated intermolecular vibrational frequencies of perfluoropentacene are also in agreement with those computed using COMPASS. However, a detailed assignment of the low-energy modes is less straightforward due to the large coupling observed with intramolecular vibrations.

Table 1. Lattice parameters of the anthracene and perfluoropentacene unit cell, as provided by the COMPASS force field and experimental X-ray diffraction data. Cell lengths are in Å.

Anthracene	*a*	*b*	*c*	α	β	γ
COMPASS	8.30	6.01	11.07	90.0°	125.6°	90.0°
Experimental[49]	8.55	6.02	11.17	90.0°	124.6°	90.0°
Perfluopentacene	***a***	***b***	***c***	α	β	γ
COMPASS	14.89	4.87	10.58	90.0°	92.2°	90.0°
Experimental[24]	15.51	4.49	11.45	90.0°	91.6°	90.0°

Table 2. Comparison between the main origin and frequency (in cm^{-1}) of the nine intermolecular modes of the anthracene unit cell at $k=0$ (Γ-point), as provided by the COMPASS force field and DFT calculations with the B3LYP functional. (S = symmetric, AS = antisymmetric).

	COMPASS	DFT	Nature
A_u	33	48	Translation axis *c* AS
A_g	43	45	Libration AS
B_g	50	48	Libration S
B_g	74	83	Libration AS
B_u	59	74	Translation axis *b* AS
A_g	85	88	Libration S
A_u	110	118	Translation axis *a* AS
B_g	145	146	Libration S
A_g	146	130	Libration AS

The influence of lattice dynamics has been further assessed by performing kinetic Monte Carlo (MC) simulations of electron transport in the anthracene and perfluoropentacene crystals with structural parameters extracted from the MD simulations and microscopic charge-transport parameters calculated at the quantum-chemical level. Since our goal here is not to provide absolute values of the charge carrier mobilities, we have considered a pure hopping regime for charge transport with the transfer rates between two neighboring molecules *i* and *j* calculated according to the simple semi-classical Marcus–Hush formulation [Eq. (3)]:[12]

$$k_{ij} = \frac{2\pi}{\hbar}|t_{ij}|^2 \frac{1}{\sqrt{4\pi\lambda k_B T}} \exp\left[-\frac{(\Delta G_{ij} - \lambda)^2}{4\lambda k_B T}\right] \quad (3)$$

Here, λ denotes the reorganization energy, t_{ij} the transfer integral, T the temperature, and ΔG_{ij} the energy difference between the initial and final states induced by the application of an external electric field [Eq. (4)]:

$$\Delta G_{ij} = q\vec{E}\,\overrightarrow{\Delta r}\,ij \quad (4)$$

with $q = +e$ ($-e$) for hole (electron) transport, $\vec{E}$ the electric field vector and $\overrightarrow{\Delta r}\,ij$ the vector between the centers of mass of the two molecular units. We have used an internal reorganization energy for electrons of 196 meV for anthracene[28] and 224 meV for perfluoropentacene,[29] as calculated previously at the DFT/B3LYP level from the adiabatic potential energy surfaces of the neutral and charged states.

The charge mobility values have been evaluated using a single-particle biased Monte Carlo algorithm in which a charge initially positioned at a random starting site performs a biased random walk under the influence of the electric field.[30] At each MC step, a hopping time for the charge at site i to hop to any of the six neighboring sites j is calculated from an exponential distribution as shown in Equation (5):

$$\tau_{ij} = -\frac{1}{k_{ij}}\ln(X) \quad (5)$$

with X a random number uniformly distributed between 0 and 1 and k_{ij} the Marcus transfer rate. The hop requiring the smallest time is selected and executed; the position of the charge and the simulation time are then updated accordingly. A transit time $\langle\tau\rangle$ averaged over ten thousand simulations is calculated for the charge migration over a distance L along the field direction. The charge carrier mobility is ultimately obtained as Equation (6):

$$\mu = \frac{L}{\tau|\vec{E}|} \quad (6)$$

for an applied field $\vec{E}$ in a given direction within the molecular layer. The charge samples a periodically repeated cell consisting of a single layer of 32 molecules.

3. Results and Discussion

Figure 2 portrays the distribution of transfer integrals for the HOMO and LUMO levels in dimer A of anthracene, that is, along the herringbone direction (see labelling of the dimers in Figure 1). This distribution has been calculated at the INDO level from 5000 snapshots generated with COMPASS. In each case, we display the transfer integrals with their actual sign as well as the squared values since the transfer integrals enter in the Marcus expression of transfer rates as squares. Note that a positive sign implies that the negative combination of the two individual levels corresponds to the most stable level (i.e. HOMO−1 level) in the dimer and *vice versa*. Similarly, we report in Figure 3 the distribution of the transfer integrals estimated at the INDO level for the LUMO of dimer A of perfluoropentacene, as extracted from 5000 MD snapshots. Periodic boundary conditions are used in all MD simulations and the

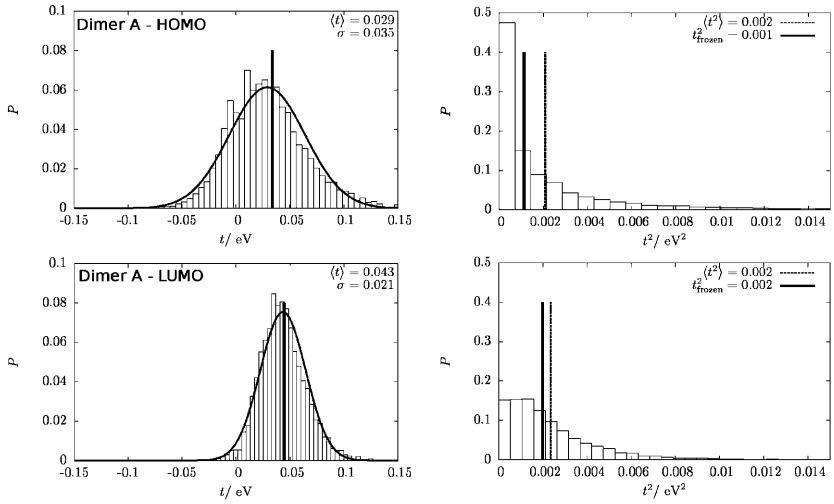

Figure 2. Probability distribution in arbitrary units of the transfer integrals for the HOMO (top) and LUMO (bottom) levels of dimer A in the anthracene unit cell, as extracted from 5000 snapshots generated with the COMPASS force field. The transfer integrals calculated at the INDO level are reported both with their proper sign (left) and with their square value (right). When justified, the distribution has been fitted with a Gaussian function; the average value $\langle t\rangle$ and the standard deviation σ are also reported.

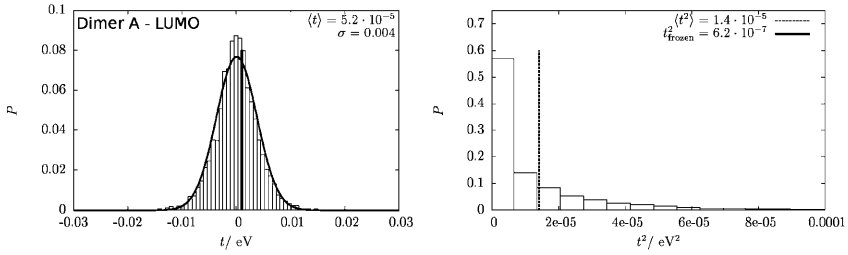

Figure 3. Probability distribution in arbitrary units of the transfer integrals for the LUMO level of dimer A in the perfluoropentacene unit cell, as extracted from 5000 snapshots generated with the COMPASS force field. The transfer integrals calculated at the INDO level are reported both with their proper sign (left) and with their square value (right). When justified, the distribution has been fitted with a Gaussian function; the average value $\langle t\rangle$ and the standard deviation σ are also reported.

size of the supercell is chosen such that the dimers of interest are surrounded by a full shell of neighboring molecules in order to prevent artificial symmetry effects (4×4×3 molecules for anthracene and 4×6×3 for perfluoropentacene).

The selected distributions of transfer integrals reported in Figures 2 and 3 allow us to identify different degrees of impact of the lattice vibrations on the charge-transport properties when compared to the equilibrium geometry. Hereafter, we distinguish among various cases by considering the ratio $\eta = |\langle t\rangle/\sigma|$, with $\langle t\rangle$ the average value of the transfer integral in the distribution (i.e. corresponding to the center of the Gaussian distribution) and σ the standard deviation of the Gaussian distribution as well as the inverse of the coherence parameter; the latter has been defined as $\langle t\rangle^2/\langle t^2\rangle$ in previous studies.[31] Note that the exact localization of the center of the Gaussian distribution is in general expected to be slightly shifted compared to the transfer integrals obtained for the equilibrium geometry of the crystal at 0 K provided by the MM calculations due to small changes in the equilibrium unit cell geometry at room temperature. When the frequency of the intermolecular modes ($\sim 10^{12}$ s^{-1} for vibrational energies of 5–20 meV) is larger than the hopping frequency, the role of the lattice vibrations can be accounted for by injecting into the Marcus rate associated to a given jump the corresponding $\langle t^2\rangle$ value, as generally done in the description of biological systems.[31] In contrast, when the frequency of the modes is smaller than the hopping frequency, each jump occurs at a rate extracted from the $\langle t\rangle^2$ distribution. These two cases can be referred to as "thermalized" and "static" limits, respectively. The actual situation often lies in between these two extreme cases in organic semiconductors. For the sake of illustration, we calculate an electron transfer rate on the order of 10^{12} s^{-1} on the basis of the Marcus-Levich-Jortner expression[32] when using typical values for the various molecular parameters in anthracene (a transfer integral of 45 meV that corresponds to the average value of the distribution for electrons, an effective intramolecular mode of 0.15 eV, and internal and external reorganization energies of 0.2 eV).

Since $\sigma^2 = \langle t^2\rangle - \langle t\rangle^2$ for a Gaussian function, we can infer Equation (7):

$$\frac{\langle t^2\rangle}{\langle t\rangle^2} = \left(\frac{1}{\eta^2} + 1\right) \tag{7}$$

When η is large (small width σ), $\langle t^2\rangle \sim \langle t\rangle^2$ and the impact of the lattice vibrations is expected to be weak. In contrast, smaller η values imply that $\langle t^2\rangle$ becomes significantly larger than $\langle t\rangle^2$ and hence that the Marcus transfer rates in the thermalized limit are globally increased by the lattice vibrations compared to the equilibrium crystal geometry. In this framework, the impact of the lattice vibrations in a given crystal can be described from the trends observed for all inequivalent dimers found in the periodic structure of the molecular crystal. We also stress that the width of the distributions reduces when the temperature is lowered (though at a larger extent than the reduction obtained with a quantum-mechanical treatment of the vibrational modes), thus indicating that the impact of thermal fluctuations is weakened and that the transport can acquire an increasing band-like character.

3.1. Case 1

The first case we consider is when the distribution is found to have almost entirely positive OR negative transfer integral values and can be fitted with a Gaussian function quasi centered on the value for the equilibrium crystal structure. This is the situation for the LUMO of anthracene, see Figure 2—bottom.[33] Note that a Gaussian broadening of the transfer integrals is expected in the framework of classical vibrations and linear electron-phonon coupling.[18] Deviations from a Gaussian function are expected when the transfer integrals do not evolve linearly along the intermolecular modes around the equilibrium geometry (thus requiring higher-order electron-phonon coupling constants).

In the case of the LUMO for anthracene pair A, $\eta = 2.1$ and $\langle t^2\rangle/\langle t\rangle^2 = 1.2$. The impact of the lattice vibrations is thus moderate owing to partial compensation between the slower and faster jumps compared to the average $\langle t\rangle$ value. In the case of anthracene, a similar distribution is obtained for all possible inequivalent dimers for electron transport, thus suggesting that globally the lattice dynamics only slightly perturbs the charge mobility values.

3.2. Case 2

This is a particular case where the transfer integral calculated for the equilibrium geometry is vanishingly small and yields a Gaussian distribution centered around zero when the lattice dynamics is included. This is the situation for the LUMO of perfluoropentacene for transport along *c*, see Figure 3. Here, $\eta = 0.01$ and translates into a huge value for the ratio $\langle t^2\rangle/\langle t\rangle^2 = 5200$. The intermolecular vibrations thus open new hopping pathways along *c*, thereby increasing the dimensionality of the charge transport in the crystal, which might prove important in the presence of structural defects. This mechanism has been referred to as conformational gating in previous electron transfer studies on donor-bridge-acceptor architectures,[34] photosynthetic reaction centers,[31] or DNA.[35] We stress that thermal fluctuations of the environment can also modulate the migration of charges, as suggested in particular for the counter-ions surrounding DNA stacks.[36,37] This scenario is easily described with Monte-Carlo simulations in the thermalized limit by injecting the proper $\langle t^2\rangle$ value for each jump. It is less straightforward in the static limit since all the inefficient jumps will prevent a fast convergence of the mobility values and will require accounting for the nuclear rearrangements if the charge is to keep propagating.[38]

3.3. Case 3

We now turn to a situation intermediate between cases 1 and 2, where the distribution of the transfer integrals has a Gaussian shape and is found to have both positive AND negative values, with the average of the Gaussian distribution matching

closely the transfer integral value characteristic of the equilibrium crystal structure. This is the case for the HOMO in dimer A of anthracene (Figure 2—top) which exhibits a much larger broadening than the LUMO despite the fact that the transfer integral values are similar for the two electronic levels in the equilibrium geometry. At first sight, the large accumulation of t^2 values around zero could lead one to consider that the transport properties in this case might be hampered by the lattice vibrations. However, since the variance of a Gaussian function σ^2 can only be positive, $\eta = 0.8$ and $\langle t^2\rangle/\langle t\rangle^2 = 2.5$, thus leading to an enhancement of the transport properties in the thermalized limit compared to the mobility values computed for the equilibrium crystal geometry.

We stress that the different impact of the lattice vibrations which we have calculated for electron *versus* hole transport in dimer A of anthracene (Figure 2) does not depend on our choice of the COMPASS force field. Similar results are obtained with other validated force fields, especially MM3. This is illustrated in Figure 4 by the distributions calculated with the MM3 force field[39] and those provided by a MD run based on a simplified force field using rigid-body constraints (NPT ensemble, $T = 300$ K, time step of 2.5 fs, see theoretical methodology section for further details), which is known to reproduce the experimental crystal structure of oligoacenes extremely well.[40]

The accumulation of t^2 values around zero can be explained by analyzing in parallel the relative displacements of the molecules during the dynamics and the corresponding evolution of the transfer integrals. Geometries leading to changes in the sign of the transfer integral are promoted efficiently in the anthracene single crystal by relative displacements along the long molecular *c* axis (see Figure 5). Note that the transfer integral is equal to zero when the amount of bonding interactions between the π-atomic orbitals in the overlapping region is exactly compensated by the amount of antibonding interactions;[8] in Figure 5, this is seen to occur at approximately 0.3 Å from the equilibrium position.

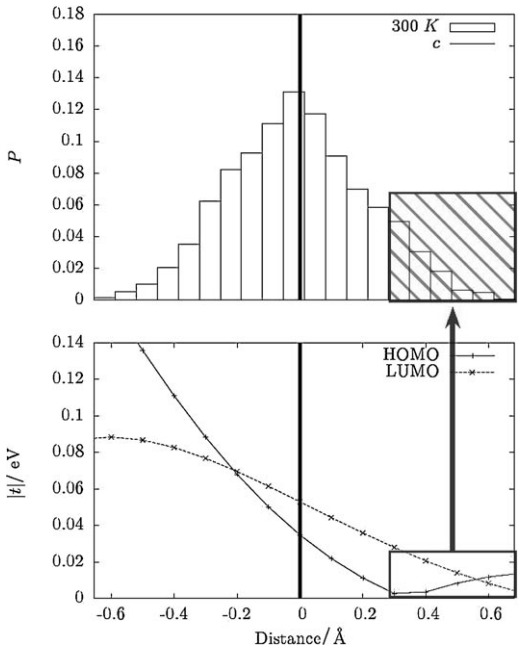

Figure 5. Top: Probability distribution in arbitrary units of the relative displacements along the *c* axis in dimer A of anthracene, as provided by a MD simulation with the COMPASS force field; Bottom: Corresponding evolution of the transfer integrals (in absolute value) for the HOMO and LUMO levels.

The relative displacements along the *c* axis of dimer A (when projected onto the *z* axis of an orthonormal system where the *x* and *y* axes correspond to the *a* and *b* crystalline axes, respectively) are fully consistent with those extracted from recent temperature-dependent X-ray diffraction data which are on the order of 0.2 Å;[41] the maximum relative displacements along the *a* and *b* axes are also on the same order. For dimer B of anthracene, values of 0.2 Å are calculated along the *b* and *c* axes and 0.3 Å along the *a* axis. Similar values are also obtained in the case of perfluoropentacene. For dimer A, maximum relative displacements are estimated to be 0.3 Å along the *a* axis and 0.15 Å along the *b* and *c* axes.

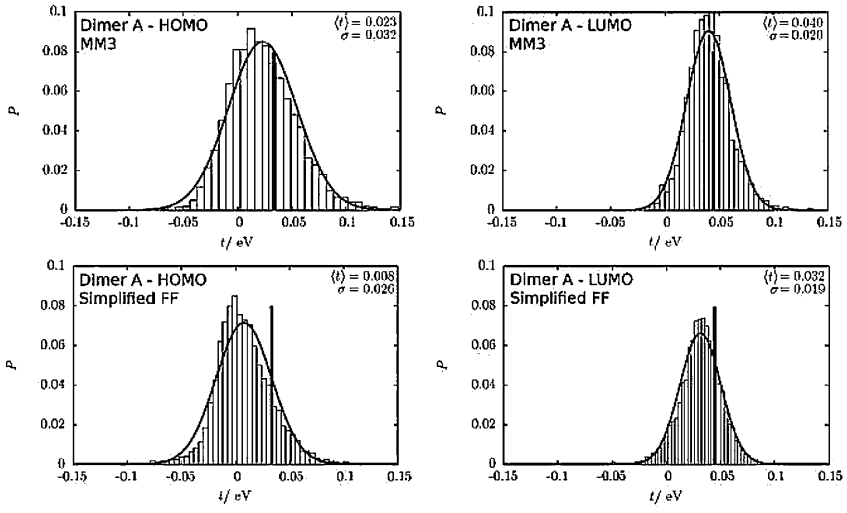

Figure 4. Probability distribution in arbitrary units of the transfer integrals for the HOMO (left) and LUMO (right) levels of dimer A of anthracene, as provided by the MM3 force field (top) and the simplified force field (bottom) using rigid-body constraints. The transfer integrals have been reported at the INDO level are reported with their proper sign. The distributions have been fitted with a Gaussian function; the average value $\langle t\rangle$ and standard deviation σ are also reported. The vertical lines correspond to the transfer integrals obtained for the equilibrium geometry at the COMPASS level.

3.4. Kinetic Monte Carlo Simulations

The impact of lattice dynamics on the charge mobility values has been further assessed by running Monte-Carlo simulations

based on Marcus transfer rates involving either : i) the square electronic coupling averaged over the MD snapshots $\langle t^2 \rangle$ for all inequivalent dimers (thermalized limit); ii) the square of the average coupling $\langle t \rangle^2$ of the dimers corresponding to the center of the Gaussian distribution and hence to the electronic coupling characteristic of the equilibrium geometry at room temperature; and iii) instantaneous t_{ij} and molecular positions for given MD configurations (static limit). The mobility is then averaged over all molecular frames (1000 MD frames separated by 30 fs). Electron transport has been considered since the LUMO distributions provide two extreme cases.

The results are summarized in Figure 6, which displays a polar plot of the electron mobility for the anthracene and perfluoropentacene crystals at $T = 300$ K for an applied electric field of 250 kV cm^{-1} (such a field is in the typical range of time of flight—TOF—experiments). For the anthracene crystal, we have calculated the two-dimensional electron mobility plot within the *a*–*b* plane. For small values of the electric field, the transport is nearly isotropic, with a small enhancement along the *a* axis direction observed for cases (i) and (ii). The plot shows that the charge carrier mobility is enhanced in the thermalized limit when replacing $\langle t \rangle^2$ by $\langle t^2 \rangle$ in Equation (3), in full consistency with the calculated η ratios equal to 1.2 and 1.5 for dimers A and B, respectively. There is an increase by ~23% along *a* and by ~6% along *b*, leading to calculated mobility values of $\mu_e = 1.74$ cm^{2}V^{-1}s^{-1} and $\mu_e = 1.70$ cm^{2}V^{-1}s^{-1}, respectively, in the hopping regime. In contrast, the charge mobility calculated in the static limit by averaging over a large number of frozen geometries in the course of the trajectory is lower than the value computed from the equilibrium structure. The same picture holds true if we calculate the mobility using the average of the transit times associated to the same distance in each snapshot. The mobility values obtained using the equilibrium structure are within the range obtained from the various individual snapshots. We note that, although our approach is not expected to provide absolute values of the mobility in these crystals, the magnitude of the calculated room-temperature electron mobility in anthracene is in good agreement with experimental values.[42–44]

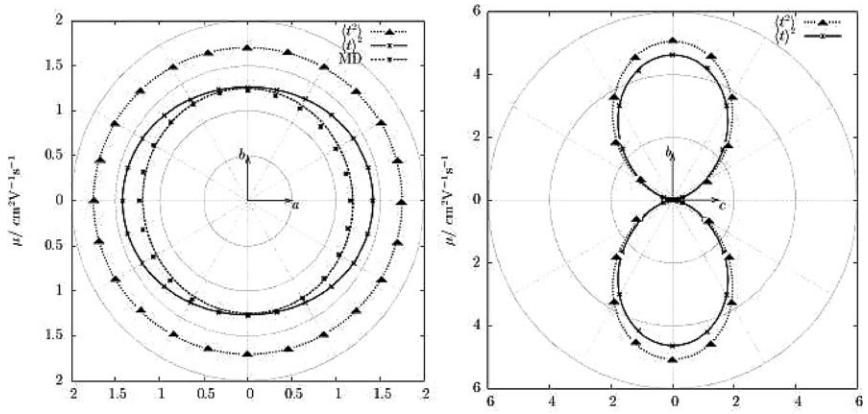

Figure 6. Polar plot of μ_e within the *a*–*b* plane for anthracene (left) and within the *b*-*c* plane for perfluoropentacene (right) crystal at $T = 300$ K and for an applied electric field of 250 kV cm^{-1}. Triangles and dotted lines refer to MC simulations using the values of $\langle t^2 \rangle$ characteristic of the equilibrium structure (thermalized limit) and crosses with solid lines to MC simulations using the values of $\langle t \rangle^2$. In the left panel, bold crosses with dotted lines are associated to mobility values averaged over all MD snapshots within a static limit.

In the case of the perfluoropentacene crystal, we observe a pronounced anisotropy in the mobility within the *b*–*c* plane that reflects the large variations in the amplitude of the electronic coupling along the different directions (see Figure 6). Electron mobility values are very low for transport along the *c* direction while the highest values are obtained for transport along the *b* axis. As in the case of anthracene, an increase in the mobility is found in the thermalized limit compared to the value characteristic of the equilibrium structure when injecting $\langle t^2 \rangle$ values in the transport simulations. This enhancement is observed for all directions within the *b*–*c* plane. In particular, we find an increase by ~45% for a deviation of 5° with respect to the *c* direction which is further substantially amplified when approaching a zero degree deviation. Though there is clearly the opening of a new conducting pathway along the *c* axis induced by lattice dynamics, transport along this direction remains strongly limited due to the two-dimensional character of the system that favors electron migration in the directions exhibiting the largest electronic couplings. In practice, it is impossible to obtain numerical results for a field applied along the *c* direction due to the vanishingly small value of the transfer rate for $\langle t \rangle^2$ compared to that along the *b* axis direction. Increasing the amplitude of the electric field up to 2000 kV cm^{-1} does not change this picture. The electron mobility increases by ~10% in the thermalized limit along the *b* axis to reach a value of 5.1 cm^{2}V^{-1}s^{-1}.

4. Conclusions

Figure 7 summarizes the three cases we have considered by plotting a graph of $\langle t^2 \rangle / \langle t \rangle^2$ versus $\eta = |<t>/\sigma|$. When consid-

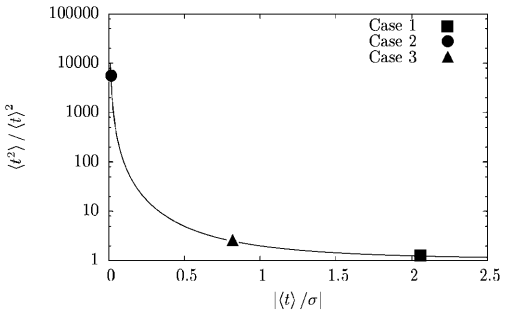

Figure 7. Illustration of the $\langle t^2 \rangle / \langle t \rangle^2$ values versus $\eta = |<t>/\sigma|$ for the three cases under study.

ering exclusively the dynamical positional disorder in a thermalized limit, the transport properties are found to be favored in all instances by lattice vibrations (compared to the properties computed for the equilibrium structure of the crystal), with an enhancement factor that depends on the actual value of η. When $\eta \geq 0.5$, the charge transport properties are only slightly influenced by the lattice vibrations and are quite insensitive to the actual value of η. When $\eta < 0.5$, the transport properties of the system are strongly affected by the lattice vibrations and small changes in η translate into large changes in the $\langle t^2 \rangle / \langle t \rangle^2$ ratio. In this case, new conduction pathways can be created in the crystal though their efficiency remains limited due to the two-dimensional character of the systems. In contrast, our simulations show that the mobility values can be lowered in the static limit.

All together, the present results point to a significant versatility in the impact of lattice vibrations on charge-transport properties, depending on the chemical nature of the organic semiconductors, their crystalline packing, the polarity of the charge carriers, and the relative timescale of lattice dynamics versus charge transfer processes. It is essential to account for these effects to yield a quantitative description of the magnitude and directionality of charge carrier transport in organic crystals. We further note that these thermal effects are not likely to be fully captured by phenomenogical models, which generally reduce the actual dimensionality of the system and/or account for only few effective intermolecular modes. We are currently extending this approach to analyze the impact of thermal fluctuations on site energies.

Computational Details

COMPASS: For anthracene, a supercell with 96 molecules is initially created via a 4×4×3 replica of the unit cell. The system has first been equilibrated during 200 ps in the NVT ensemble (using an Andersen thermostat) with a timestep of 1 fs. We have then run a simulation of 150 ps to extract 5000 frames separated by a time interval of 30 fs to have a good statistical description of the dynamics. For perfluoropentacene, a supercell with 144 molecules was constructed from a 4×6×3 replica of the unit cell. The system was equilibrated for 180 ps (using an Andersen thermostat) in the NVT ensemble and a timestep of 1 fs. After the equilibration, a simulation of 150 ps was run and 5000 frames were extracted every 30 fs along the trajectory.

MM3: The anthracene crystal unit cell was replicated to build a 4×4×3 supercell containing 96 molecules. Molecular dynamics (MD) simulations were carried out at 300 K in the canonical NVT ensemble with a timestep of 1 fs, using the computer code TINKER.[45,46] A cutoff of 10 Å was adopted when evaluating both van der Waals and electrostatic interactions. The simulations lasted 150 ps and atomic coordinates were saved every 30 fs (i.e. 5000 frames), after an equilibration period of 150 ps, to be used as input in the quantum-chemical calculations.

Simplified Force Field: We used for anthracene a force field with the intermolecular interactions described by a pairwise additive atom-atom potential of the form $V_{ij}(r) = A_{ij} \exp(-B_{ij}r) - C_{ij}/r^6 + q_i q_j / r$, which combines a Buckingham potential model with a Coulombic contribution described by atomic charges q_i. The Buckingham parameters were given by Williams parameter set IV for C and H atoms.[47] A supercell with 120 molecules has been created as an 4×5×3 replica of the unit cell. The system has been equilibrated during 2 ns in the NPT ensemble (with a Nosé-Hoover barostat-thermostat, $T = 300$ K and $P = 0$ GPa) with a timestep of 2.5 fs. The cell is here constrained to remain monoclinic and rigid-body conditions are used, thus neglecting the coupling between the intermolecular modes and the low-frequency intramolecular modes which is active in the COMPASS and MM3 simulations. After the equilibration period, 5000 frames are recorded at time intervals of 30 fs for the dynamical analysis.

Crystal: The calculation of the intermolecular vibrational frequencies was done at the Γ-point using the hybrid B3LYP functional and Gaussian basis sets, as implemented in the ab initio CRYSTAL06 package.[48] The 6-31G basis set and an uniform 8×8×8 Monkhorst-Pack *k*-point mesh were employed here.

Acknowledgements

We acknowledge very stimulating discussions with Dr. V. Coropceanu (Georgia Institute of Technology). The work in Mons is partly supported by the Belgian Federal Governement "Interuniversity Attraction Pole in Supramolecular Chemistry and Catalysis, PAI 5/3"; Région Wallonne (Project ETIQUEL); the European project MODECOM (NMP3-CT-2006-016434) and the European Community's Seventh Framework Programme (FP7/2007-2013) under grant agreement 212311 for the ONE-P project; and the Belgian National Fund for Scientific Research (FNRS/FRFC). The work at Georgia Tech is partly supported by the National Science Foundation (STC Program under Award DMR-0120967, MRSEC Program under Award DMR-0212302, and CRIF Program under Award CHE-0443564). J.C. and D.B. are FNRS Research Fellows; N.M. and Y.O. acknowledge a grant from "Fonds pour la Formation à la Recherche dans l'Industrie et dans l'Agriculture (FRIA)". M.C.R.D. is grateful to the MEC/Fulbright for her Postdoctoral Fellowship at the Georgia Institute of Technology.

Keywords: acenes · electron-transfer process · molecular crystals · molecular dynamics · molecular mechanics

[1] N. Karl, *Synth. Met.* **2003**, *133*, 649.
[2] H. Bässler, *Phys. Status Solidi B* **1993**, *175*, 15.
[3] Y. C. Cheng, R. J. Silbey, *J. Chem. Phys.* **2008**, *128*, 114713.
[4] A. Troisi, *Adv. Mater.* **2007**, *19*, 2000.
[5] A. Troisi, G. Orlandi, *J. Phys. Chem. A* **2006**, *110*, 4065.
[6] A. Troisi, G. Orlandi, J. E. Anthony, *Chem. Mater.* **2005**, *17*, 5024.
[7] J. L. Brédas, D. Beljonne, V. Coropceanu, J. Cornil, *Chem. Rev.* **2004**, *104*, 4971.
[8] J. L. Brédas, J. P. Calbert, D. A. da Silva Filho, J. Cornil, *Proc. Natl. Acad. Sci. USA* **2002**, *99*, 5804.
[9] M. A. Ratner, A. Madhukar, *Chem. Phys.* **1978**, *30*, 201.
[10] K. Hannewald, P. A. Bobbert, *Appl. Phys. Lett.* **2004**, *85*, 1535.
[11] L. J. Wang, Q. Peng, Q. K. Li, Z. Shuai, *J. Chem. Phys.* **2007**, *127*, 044506.
[12] R. A. Marcus, *Rev. Mod. Phys.* **1993**, *65*, 599.
[13] V. Coropceanu, J. Cornil, D. A. da Silva Filho, Y. Olivier, R. Silbey, J. L. Brédas, *Chem. Rev.* **2007**, *107*, 926.
[14] Y. Olivier, V. Lemaur, J. L. Brédas, J. Cornil, *J. Phys. Chem. A* **2006**, *110*, 6356.
[15] J. Kirkpatrick, V. Marcon, J. Nelson, K. Kremer, D. Andrienko, *Phys. Rev. Lett.* **2007**, *98*, 227402.
[16] F. C. Grozema, L. D. A. Siebbeles, *Int. Rev. Phys. Chem.* **2008**, *27*, 87.

[17] A. Troisi, A. Nitzan, M. A. Ratner, *J. Chem. Phys.* **2003**, *119*, 5782, and references cited therein.
[18] V. Coropceanu, R. S. Sànchez-Carrera, P. Paramonov, G. M. Day, J. L. Brédas, *J. Phys. Chem. C* **2009**, *113*, 4679.
[19] M. Oehzelt, A. Aichholzer, R. Resel, G. Heimel, E. Venuti, R. G. Della Valle, *Phys. Rev. B* **2006**, *74*, 104103.
[20] M. Suzuki, T. Yokohama, M. Ito, *Spectrochim. Acta Part A* **1968**, *24*, 1091.
[21] K. Senthilkumar, F. C. Grozema, F. M. Bickelhaupt, L. D. A. Siebbeles, *J. Chem. Phys.* **2003**, *119*, 9809.
[22] E. F. Valeev, V. Coropceanu, D. A. da Silva Filho, S. Salman, J. L. Brédas, *J. Am. Chem. Soc.* **2006**, *128*, 9882.
[23] J. Ridley, M. C. Zerner, *Theor. Chim. Acta* **1973**, *32*, 111.
[24] Y. Sakamoto, T. Suzuki, M. Kobayashi, Y. Gao, Y. Fukai, Y. Inoue, F. Sato, S. Tokito, *J. Am. Chem. Soc.* **2004**, *126*, 8138.
[25] J. R. Ferraro, K. Nakamoto, C. W. Brown, *Introductory Raman Spectroscopy, 2nd ed.*, Academic Press, London, **2003**.
[26] S. W. Bunte, H. Sun, *J. Phys. Chem. B* **2000**, *104*, 2477.
[27] A. K. Rappe, C. J. Casewit, K. S. Colwell, W. A. Goddard, W. M. Skiff, *J. Am. Chem. Soc.* **1992**, *114*, 10024.
[28] I. A. Balabin, J. N. Onuchic, *Science* **2000**, *290*, 114.
[29] A Chi square test has been performed on each plot to validate the use of a Gaussian fit; see *Statistics* by R. Pisani and R. Purves, W. W. Norton, 4th edition, **2009** New York
[30] P. F. Barbara, T. J. Meyer, M. A. Ratner, *J. Phys. Chem.* **1996**, *100*, 13148.
[31] W. B. Davis, M. A. Ratner, M. R. Wasielewski, *J. Am. Chem. Soc.* **2001**, *123*, 7877.
[32] A. Troisi, G. Orlandi, *J. Phys. Chem. B* **2002**, *106*, 2093.
[33] R. N. Barnett, C. L. Cleveland, A. Joy, U. Landman, G. B. Schuster, *Science* **2001**, *294*, 567.
[34] A. A. Voityuk, K. Siriwong, N. Rösch, *Angew. Chem.* **2004**, *116*, 634; *Angew. Chem. Int. Ed.* **2004**, *43*, 624.
[35] M. Hultell, S. Stafström, *Chem. Phys. Lett.* **2006**, *428*, 446.
[36] a) N. L. Allinger, Y. H. Yuh, J. H. Lii, *J. Am. Chem. Soc.* **1989**, *111*, 8551; b) J. H. Lii, N. L. Allinger, *J. Am. Chem. Soc.* **1989**, *111*, 8566 and J. H. Lii, N. L. Allinger, *J. Am. Chem. Soc.* **1989**, *111*, 8576.
[37] R. G. Della Valle, E. Venuti, A. Brillante, A. Girlando, *J. Phys. Chem. A* **2006**, *110*, 10858.
[38] S. Haas, B. Batlogg, C. Besnard, M. Schiltz, C. Kloc, T. Siegrist, *Phys. Rev. B* **2007**, *76*, 205203.
[39] V. Coropceanu, M. Malagoli, D. A. da Silva Filho, N. E. Gruhn, T. G. Bill, J. L. Brédas, *Phys. Rev. Lett.* **2002**, *89*, 275503.
[40] M. C. R. Delgado, K. R. Pigg, D. A. da Silva Filho, N. E. Gruhn, Y. Sakamoto, T. Suzuki, R. M. Osuna, J. Casado, V. Hernández, J. T. L. Navarrete, N. G. Martinelli, J. Cornil, R. S. Sánchez-Carrera, V. Coropceanu, J. L. Brédas, *J. Am. Chem. Soc.* **2009**, *131*, 1502.
[41] S. Athanasopoulos, J. Kirkpatrick, D. Martínez, J. M. Frost, C. M. Foden, A. B. Walker, J. Nelson, *Nano Lett.* **2007**, *7*, 1785.
[42] R. G. Kepler, *Phys. Rev.* **1960**, *119*, 1226.
[43] T. Kajiwara, H. Inokuchi, and S. Minomura, *Bull. Chem. Soc. Jpn.* **1967**, *40*, 1055.
[44] N. Karl, . Marktanner, *Mol. Cryst. Liq. Cryst.* **2001**, *355*, 149.
[45] J. W. Ponder, TINKER: Software Tools for Molecular Design, 4.2 ed., Washington University School of Medicine: Saint Louis, MO, **2004**.
[46] a) P. Ren, J. W. Ponder, *J. Phys. Chem. B* **2003**, *107*, 5933; b) P. Ren, J. W. Ponder, *J. Comput. Chem.* **2002**, *23*, 1497; c) R. V. Pappu, R. K. Hart, J. W. Ponder, *J. Phys. Chem. B* **1998**, *102*, 9725; d) M. E. Hodsdon, J. W. Ponder, D. P. Cistola, *J. Mol. Biol.* **1996**, *264*, 585; e) C. E. Kundrot, J. W. Ponder, F. M. Richards, *J. Comput. Chem.* **1991**, *12*, 402; f) J. W. Ponder, F. M. Richards, *J. Comput. Chem.* **1987**, *8*, 1016.
[47] D. E. Williams, *J. Chem. Phys.* **1967**, *47*, 4680.
[48] R. Dovesi, V. R. Saunders, C. Roetti, R. Orlando, C. M. Zicovich-Wilson, F. Pascale, B. Civalleri, K. Doll, N. M. Harrison, I. J. Bush, P. D'arco, M. Llunell, CRYSTAL06 User's Manual, University of Torino, Torino, **2006**.
[49] C. P. Brock, J. D. Dunitz, *Acta Crystallogr. Sect. B* **1990**, *46*, 795.

Received: April 17, 2009
Published online on July 27, 2009

